Quantification of biochar content in a natural soil by spectral induced polarization: a laboratory experiment

Aida Mendieta[1], Julien Thiesson[1], Alexis Maineult[1], Haoliang Luo[1], Damien Jougnot[1], Marco D. Vásconez-Maza[1,2], Cécile Finco[3], Frédéric Delarue[1]

[1]Sorbonne Université, CNRS, EPHE, UMR 7619 METIS, 75005 Paris, France

[2]Department of Mining and Civil Engineering, Universidad Politécnica de Cartagena, Paseo Alfonso XIII, 52, 30203 Cartagena, Murcia, Spain

[3]Univ Rouen Normandie, UNICAEN, CNRS, M2C UMR 6143, F-76000 Rouen, France

Corresponding author: Aida Mendieta, aida.mendieta_tenorio@sorbonne-universite.fr

Abstract

Biochar garners significant attention due to its relevance in the realms of environmental sustainability, archaeology, and agronomy. However, monitoring the fate of biochar in soils remains challenging. Environmental geophysics characterizes the near surface non-intrusively to better understand the subsurface's hydro-bio-geo-chemical processes. Hence, spectral induced polarization (SIP) has been proposed as a potential method to characterize biochar content in soils. Thus far, only highly controlled laboratory experiments have been carried out with sand and biochar. Here, we present SIP measurements of a natural soil, in which biochar was incorporated at different mass proportions: 0, 0.1, 1, 5, and 10%. Strong relationships between SIP derived parameters and biochar content were found. Interestingly, we observe that simple curve descriptors such as the phase at 11.7 Hz and the shape parameter α (height of a triangle defined by a peak in the phase) were enough and suitable to detect biochar content in the studied soil. Overall our study suggests that SIP can quantify biochar content in the laboratory under controlled soil moisture conditions.

1 Introduction

Biochar is the by-product of plant biomass pyrolysis (Roberts et al., 2010; Lehmann & Joseph, 2015). Biochar has been suggested as a mean to provide agronomic and environmental benefits including bioenergy production, increase in water retention, reduction of nutrient leaching, increase of crop productivity and mitigation of greenhouse gas emissions through its incorporation into soils (Woolf et al., 2010; J. Wang & Wang, 2019). The role of biochar to mitigate climate change is mainly attributed to its high degree

of aromaticity limiting biological and abiotic degradation favouring in turn, carbon storage into soils (Xu et al., 2021). Although, persistence of biochar in soil depends on its intrinsic properties (such as large specific surface area, abundant functional groups, and developed pores, Lehmann et al., 2009), it also depends on soil properties (e.g. texture, clay mineralogy, native soil carbon content; Yang et al., 2022); plant inputs (Hammes & Schmidt, 2009), and environmental factors such as moisture and temperature (Joseph et al., 2021). If a low portion of biochar seems prone to microbial degradation (Palansooriya et al., 2019), biochar can also be lost via lateral movement or downward migration in the soil as a consequence of coarse texture and/or bioturbation (Zhang et al., 2010). Up to now, responses of biochar to degradation and downward migration remain poorly documented in the field (Singh et al., 2015). Hence, long-term effect of biochar on soil properties remains an open question. There are significant efforts to better understand these processes, however better tools to characterize the presence and effect of biochar in a soil are needed. That is, an accurate quantification of biochar in soils is required in order to characterize their spatial and temporal dynamics at the field scale (Gao et al., 2017; Mukherjee et al., 2021).

Charred particles counting (Rhodes, 1998; Lesven et al., 2022), chemical oxidation followed by elemental analyses (Gustafsson et al., 1997; Knicker et al., 2008), Ultra-Violet oxidation followed by solid-state ^{13}C nuclear magnetic resonance (Skjemstad et al., 1996), thermal degradation (Nakhli et al., 2019; Hardy et al., 2022), spectroscopy (Paetsch et al., 2017) and acid digestion followed by the quantification of benzenepolycarboxylic acids (Brodowski et al., 2005; Glaser et al., 1998) are among the main methods used to quan-

tify the biochar content in soil. All these methods require preliminary sampling, which intrinsic limitations (e.g. quantity of analysed soil or accuracy in determining the investigated depth) can hamper our ability to detect a few but significant changes in biochar degradation and/or migration. Because of their "invasive" nature, these methods are also not suitable to provide a continuous monitoring of the spatial and temporal dynamics of biochar in soil.

Geophysical methods are known to provide reliable information on soil properties at the field scale (Robinson et al., 2008; Hermans et al., 2023), in a non-invasive way, particularly electric and electromagnetic methods (see Friedman, 2005; Parsekian et al., 2015; Binley & Slater, 2020), such as electrical resistivity tomography (ERT, Samouëlian et al., 2005), electromagnetic induction (EMI, Benech et al., 2016; Tabbagh et al., 2021), or induced polarization methods in the time or frequency domain (see Kemna et al., 2012). Among geo-electrical (induced polarization) methods, spectral induced polarization (SIP) has been suggested as a valuable tool to detect and monitor biochar in soil (e.g., Haegel et al., 2012; Gurin et al., 2014; Gao et al., 2017, 2019). SIP informs about the ability a geo-material has to conduct electricity and polarize itself electrically. Gao et al. (2017) mentions that biochar polarizes similarly to conductive or semi-conductive materials. Metallic and semi-conductors give rise to an electric polarization when an external electrical field is imposed and the charge-carriers move according to the sinusoidal electrical field (see Mao & Revil, 2016).

Following this, Gao et al. (2017, 2019) suggested that SIP derived parameters were related to the content of biochar in sand-biochar mixtures. Nonetheless, this pioneering

investigation was designed to evaluate the effect of the interaction between water saturation and two biochar concentrations (1 and 2 %) on SIP signatures rather than evaluating SIP signatures as a mean to quantify biochar concentrations. Although these studies paved the way for the application of SIP to monitor the spatial and temporal dynamics of biochar in soil, several intermediate steps are still required before a field application. First, if sand presents numerous advantages from an experimental point of view, it is not representative of the complex texture of natural soils with sand, silt and clay-sized mineral particles, that have their own SIP response (Mendieta et al., 2021). Second, the SIP response to the amendment of biochar was tested using two low concentrations (1 and 2 wt%, Gao et al., 2019) implying that additional experiments are required to assess the overall potential of SIP as a mean to quantify biochar content in soils. In this study our aim is therefore to test the potential of SIP to quantify a wide range in biochar content in a natural soil with simple and traditional geophysical parameters with the use of three replicates.

2 Materials and methods

2.1 Sample preparation

The soil used in the samples came from a test site located at the CEREMA (Centre for Studies and Expertise on Risks, the Environment, Mobility and Urban Planning) near the city of Rouen, France. The cationic exchange capacity (CEC) of the soil was measured by blue methylene tests which give an average value of 3.12 $\pm$ 0.36 g/100g eq. It means that the utilized soil has small reactive content. It was then determined, by gran-

ulometry that this soil contains, on average 19.9 ± 5.5 % clay, 69.8 ± 6.4 % silt, and 10.3 ± 3.7% sand.

Firstly, the soil was dried at a temperature of 40 °C, during 10 days. Pyrolitic biochar was used in this experiment. Afterwards, we crushed separately both biochar (74.08% C, 0.72% N, and 3% H) and soil and sifted them to a grain size lower than 2 mm. Later, the dry soil and biochar were mixed with an electric drill, obtaining mass proportions of biochar content of: 0%, 0.1%, 1%, 5%, and 10%. Following, a mixing of de-ionized water, biochar and soil was done with an electric drill. The mass water content of all samples was set at 27.5%. The choice of this water content value allows for a good plasticity to fill the non-watertight sample holder (see Mendieta et al., 2021, 2023, for details on the choice of sample holder). The decision on using de-ionized water was made because the soil samples had not been flushed, thus the original ions present in the soil remained. After adding water and a period of 24 h, we placed the wet sample in the sample holder. Three separate batches (replicates) were made, this is not an usual practice in SIP studies but it is in soil science studies.

2.2 Spectral induced polarization

The SIP measurements were performed with the SIP-FUCHS III (Radic Research, www.radic-research.de).

For the SIP measurement and with the SIP-FUCHS III, a sinusoidal potential difference is imposed between a pair of electrical current injection electrodes. A resulting potential difference is measured in a different pair of electrical potential measuring elec-

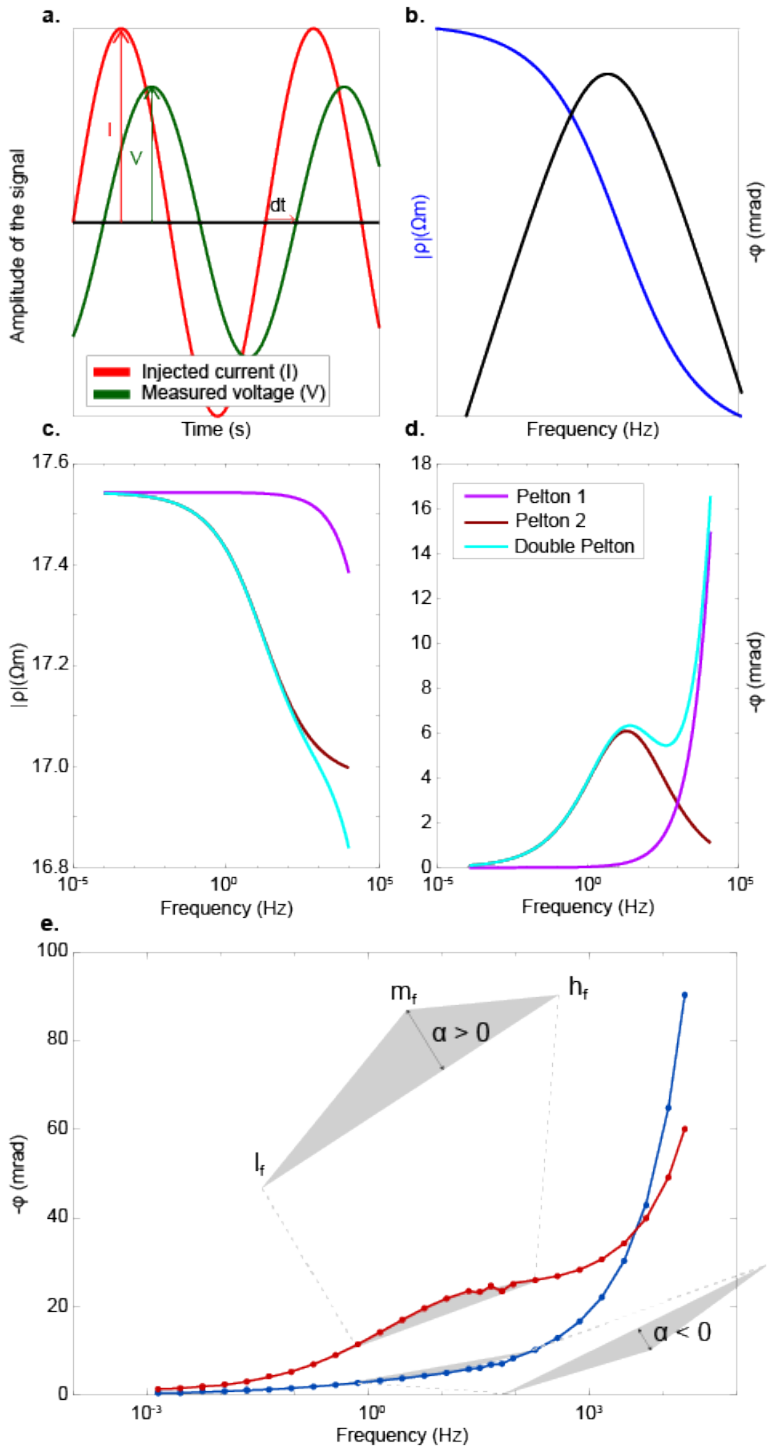

Figure 1. a) Principle of the injection of an electrical current and its voltage response at a single frequency. b) The amplitude of the resistivity and phase at multiple frequencies. Schematic of a double Pelton model from the (c) amplitude of the resistivity and (d) the phase, with 2 single Pelton models and a double-Pelton model that is the sum of the previous single Pelton models. (e) Concept of the parameter α.

trodes. Before starting the measurements over the full frequency range (1 mHz to 20 kHz), short tests are performed to adapt the imposed input electric potential difference (1 Hz to 20 kHz). A very low potential difference yield poor quality data (low signal-to-noise ratio), and a very high potential difference could be out of the validity of Ohm's law (linearity). In this case, for the whole dataset the range of injected electrical current is from 0.1 to 0.05 mA, yielding measurement errors below 1%.

Following this, SIP yields information about the electrical resistivity (ρ or its inverse, the electrical conductivity σ) and polarization through the amplitude of the measured electrical potential difference and injected current and the phase-lag (in mrad) between them (see figure 1a) at different frequency values (figure 1b).

Previous SIP biochar experiments (see Gao et al., 2017, 2019) have been carried out with sand and biochar mixtures. The polarization of silica sand is thought to be mainly from the Stern layer polarization and very small (i.e., negligible); hence the presence of biochar could clearly and undoubtably be highlighted. Natural soils being a mixture of clays, sands, water, among others make difficult to interpret their SIP response. Nevertheless according to Revil et al. (2017) it is possible to model the SIP response of a polarizing background (silty soil for this study) and add the polarization of an inclusion (biochar in this study).

2.3 Data pre-processing and Pelton model adjustment

First, the correction proposed by Florsch et al. (2014) was applied to the SIP measured data (see figure 2 c and d) to remove the high frequency noise. Second, we per-

formed an optimization procedure (following Maineult, 2016) that allows us to obtain the Pelton parameters.

Pelton-type models (see figure 1c and d) are empirical and allow to describe a SIP curve with few parameters (Ghorbani et al., 2009). Such models consist of at least the four following parameters: the direct current resistivity ρ_0 (in Ωm, or its inverse σ_0 in S m^{-1}), the chargeability m (mV/V), the Cole-Cole exponent c (no units), and the relaxation time τ (in s). ρ_0 informs about the resistance of a material to an electrical current, m about the capacity of a material to store charges reversely, τ determines the characteristic time at which a material electrically discharges itself, and c is a constant that informs about the distribution of relaxation times of a material (for more information see Tarasov & Titov, 2013; Revil et al., 2012). A single Pelton model describes a single polarization peak of a material (that is a singular cause for polarization). In this work we use a double Pelton model (i.e., two polarization peaks), one peak describing the polarization of biochar at lower frequencies and one describing the high frequency behaviour (see figure 1 c and d). The equation that describes the double-Pelton model is:

$$\rho^*(\omega) = \rho_0 \left[1 - m_1 \left(1 - \frac{1}{1 + (i\omega\tau_1)^{c_1}}\right) - m_2 \left(1 - \frac{1}{1 + (i\omega\tau_2)^{c_2}}\right)\right], \tag{1}$$

where $\rho^*(\omega)$ is the complex and frequency dependent electrical resistivity (in Ωm). Note that the subscripts 1 and 2 correspond to the Pelton for the the low and high frequency polarizations, respectively. The high frequency peak contains both the polarization of the material and a high frequency capacitive effect which may have a component linked

to the electromagnetic coupling of the cables (which has no interest in the present study). For a four-electrode system this effect is normal (see Kemna et al., 2012).

2.4 Curve parametrization from the polarization spectra

In addition to Pelton derived parameters, we defined simple characterization parameters, such as: the phase at 11.7 Hz, the resistivity at 11.7 Hz, and the average phase at a mid-frequency range (1.46 - 46.88 Hz). The frequency of 11.7 Hz was chosen because the maximum of the phase curve is at 11.7 Hz.

As an attempt to characterize the effect of biochar on SIP measurements we introduce the shape parameter α. We define it as the height of a triangle located in a the phase spectrum. The height of the triangle can be measured graphically or numerically, we propose an analytical solution in Appendix 1. The triangle is constructed from three points in the curve, given by its inflection points. That is, one point at a low, medium and high frequencies (lm, mf, and hf, respectively), with the medium point at a maximum or minimum of the curve (see figure 1e). A positive value of α denotes a downward concavity and on the contrary a negative value represents an upward concavity. An α value of zero represents a straight line, that is the lack of a peak in the chosen frequency range of the phase plot.

3 Results and discussion

Up until now SIP has been tested on mixtures of sand and biochar (Gao et al., 2017, 2019). However, natural soils have a complex texture, including sand, silt, and also clay

which also has its own significant SIP signature (see for instance, Revil et al., 2012; Mendieta et al., 2021, among others).

When a mineral is in contact with an electrolyte, an electrical charge builds up in its surface, creating an electrical double layer (EDL). When subjecting these EDL containing systems (e.g., soils) to an external electrical field, the EDL polarizes. EDL polarization happens at around the Hz frequency (Loewer et al., 2017) which is in the range expected for biochar (Gao et al., 2017). It is then important to test if the presence of clay interferes with the SIP signature of biochar. In the present study, we show that the presence of biochar can indeed be detected by SIP despite the presence of clay. This was observed (1) according to its correlation between the amplitude of the resistivity and the phase with biochar content; and (2) following the evolution of the shape of the phase curves with biochar content.

As mentioned by Gao et al. (2017), biochar acts as conductors or semi-conductors, it was then expected that with an increase of its content the electrical resistivity of the measured media decreases. Similarly, for the measured phase, an increase of the phase value is expected with an increase of the weight fraction of biochar (see Revil et al., 2017).

The sample with the highest biochar content (10% wt.) has the lowest resistivity (41.43 Ωm at 11.7 Hz) and conversely the sample without biochar presents the highest resistivity values (69.12 Ωm at 11.7 Hz, figures 2a and c). In addition to changes of the SIP signature at low and medium frequencies, an increase of the phase at the highest frequencies (above 1 kHz) was observed (figure 2b). Figures 2 c and d describe the evolution of the amplitude of the resistivity and the phase as a function of frequency of soil

biochar mixtures, with the high frequency correction. We observe a peak in the phase near 10 Hz for the soils in which, 5 and 10% of biochar were incorporated (figures 2b and d). The amplitude of this peak decreases with biochar content. It is worth mentioning that the phase at high frequencies comes from both polarization of the sample and a capacitive effect linked to the electromagnetic coupling (see Zimmermann et al., 2008).

The traditional way to interpret SIP curves is through physical models or phenomenological (notably Pelton type models, see for instance, Tarasov & Titov, 2013; Leroy et al., 2017; Weller & Slater, 2022), here applied to SIP curves corrected from high frequency noise (figures 2 c and d).

A double-Pelton model is able to represent a double-peaked SIP dataset with seven parameters (ρ_0, m_1, τ_1, c_1, m_2, τ_2, and c_2, see eqn.1). The high frequency peak is determined by the Pelton parameters presenting the subscript 1, while the peak near 10 Hz is defined according to the parameters with the subscript two (following figure 1 c and d). Table 1 presents the fitted Pelton parameters for both peaks and their correlation coefficient with biochar. In the following, we will focus on peak 2 (near 10 Hz) where Gao et al. (2017) already observed an effect of biochar. Overall, we verify that the resistivity (ρ_0) decreases with an increase of biochar content (70.2 to 43.6 Ωm). Additionally, the chargeability (m_2) increases with biochar content (0.066 to 0.114 mV/V), as the relaxation time (τ_2, 3.80×10^{-4} to 7.01×10^{-3} s), and the Cole-Cole exponent (c_2, 0.334 to 0.436).

In addition to double-Pelton parameters, we introduce three other parameters, namely the mean phase in the medium frequency range ($\bar{\varphi}_{MF}$), the phase at 11.7 Hz and the

parameter α, all determined on the uncorrected and corrected data (see figure 1e). The choice of focusing in the mid-frequency region(1.46 to 46.88 Hz) was made because it is both where the polarization peak presents itself, and because this frequency range is within a typical frequency range that could be used in a field campaign (see Martin et al., 2021). A high correlation coefficient (0.99-0.97) was determined between the biochar content and these three parameters (see figure 3). Interestingly, the phase measured at 11.7 Hz on an uncorrected spectra constitutes the best descriptor of biochar content ranging between 0 and 10 % (wt.%). These results show that the double-Pelton model and the removal of the high frequency noise can be avoided to determine biochar content as a function of the SIP signature. Hence, our simplistic but reliable approach (phase at 11.7 Hz) opens the possibility to track biochar content with SIP through a new routine that can be useful in soil science.

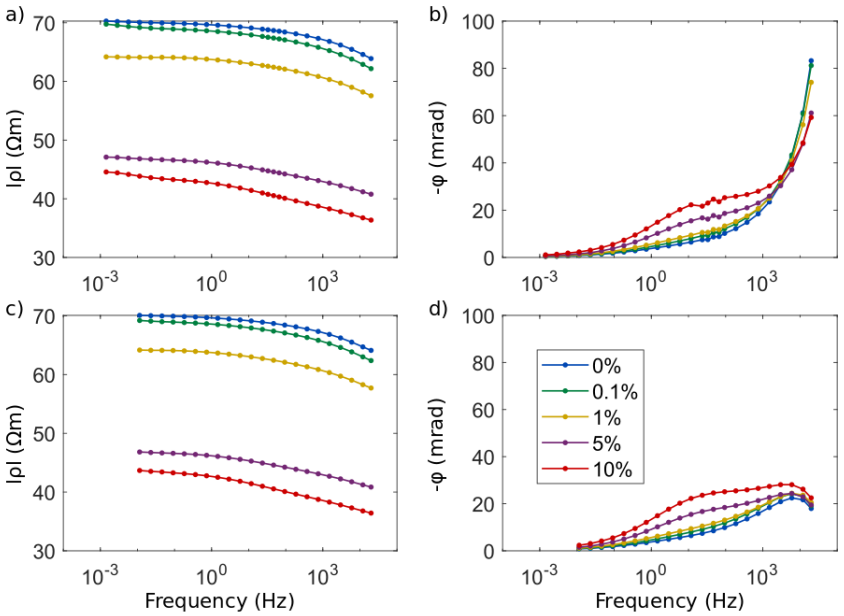

Figure 2. a) Average (n=3) amplitude of the resistivity from the soil-biochar mixtures. b) Average (n=3) phase from the soil and biochar samples. c) Average (n=3) corrected amplitude of the resistivity from the soil and biochar samples. d) Average (n=3) corrected phase from the soil-biochar mixtures.

Table 1. Fitted Pelton parameters, presented in average and its standard deviation. The last row presents Pearson's correlation (between biochar content and its corresponding parameter).

biochar (%)	ρ_0 (Ωm)	m_1 (mV/V)	τ_1 (s)	c_1 (-)	m_2 (mV/V)	τ_2 (s)	c_2 (-)
0	70.2 ± 1.7	0.042 ± 0.006	$2.37\times10^{-5}\pm 2.04\times10^{-6}$	0.752 ± 0.037	0.066 ± 0.013	$3.80\times10^{-4}\pm 1.30\times10^{-4}$	0.334 ± 0.004
0.1	69.2 ± 1.9	0.043 ± 0.003	$2.48\times10^{-5}\pm 1.67\times10^{-6}$	0.747 ± 0.007	0.078 ± 0.003	$5.07\times10^{-4}\pm 2.24\times10^{-4}$	0.336 ± 0.010
1	64.4 ± 5.8	0.055 ± 0.013	$2.14\times10^{-5}\pm 1.27\times10^{-6}$	0.681 ± 0.046	0.072 ± 0.007	$1.50\times10^{-3}\pm 9.59\times10^{-4}$	0.357 ± 0.008
5	46.8 ± 1.2	0.065 ± 0.013	$2.55\times10^{-5}\pm 4.06\times10^{-6}$	0.618 ± 0.057	0.084 ± 0.003	$5.30\times10^{-3}\pm 1.67\times10^{-3}$	0.427 ± 0.010
10	43.6 ± 3.2	0.075 ± 0.010	$2.72\times10^{-5}\pm 3.47\times10^{-6}$	0.583 ± 0.046	0.114 ± 0.010	$7.01\times10^{-3}\pm 2.28\times10^{-3}$	0.436 ± 0.021
r	-0.92	0.81	0.50	-0.83	0.89	0.90	0.91

Beyond the correlation between the SIP derived parameters and the biochar content, the parameter α can identify the presence of biochar above 5% (0.33 $\pm$ 0.09) in content within a natural soil sample (-0.48 $\pm$ 0.10). Between 0 and 1% the value of α is negative, while above 5% it is positive. Thus, we could infer that the approach presented in this paper could be an useful tool to find potential biochar hot-spots in the field with simple to obtain parameters (e.g.: positive α values).

It is important to emphasize that the source of the SIP signature arises from the whole mixture, that is: soil, water and biochar. Indeed, variable water content, soil texture, feedstocks, carbonization degree (depending on temperature and residence time), biochar particle size, additional carbon inputs into soils (from plant and microbial biomass) and biochar aging can conspicuously modify the SIP signature of biochar; according several conduction paths such as the pore structure (and pore water).

In this study, we investigated the quantification of the biochar content by SIP under controlled laboratory conditions. The diversity in soil properties, water content as well as the physical and chemical structure of biochar are not considered here although it can play a key role in the field on the response of SIP signatures. Soil can contain organic matter (e.g., litter, plant roots,bacteria, fungi,...). Several studies also entail the impact of organic matter on SIP signatures (e.g.: Schwartz et al., 2014; Mellage et al., 2022; Strobel et al., 2023). In addition, activity of below ground life can also alter the SIP response (see more in Atekwana & Slater, 2009; Kessouri et al., 2019). One of the main electrical conduction and polarization paths is through the pore water and its interface with minerals. Therefore, water content can highly impact the SIP response in

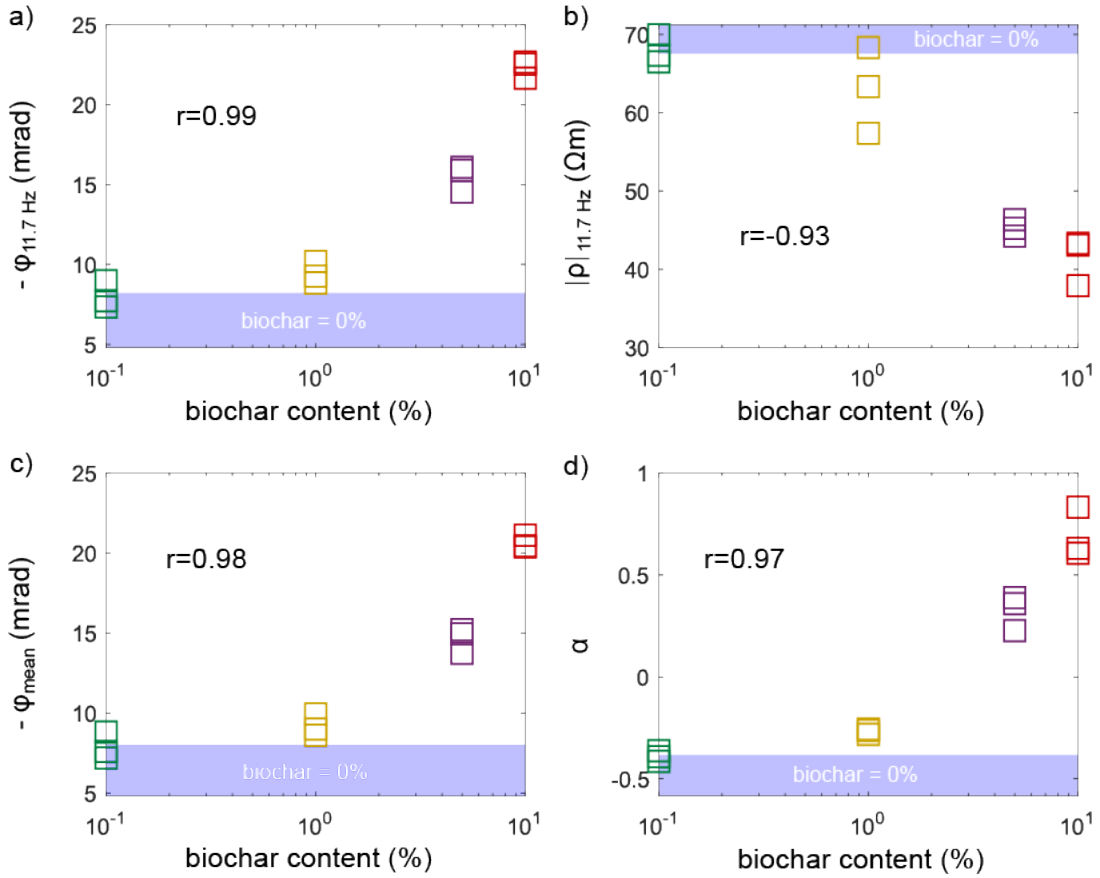

Figure 3. (a) The phase at 11.7 Hz, (b) the resistivity at 11.7 Hz, (c) the average phase at a medium frequency range, and (d) the parameter α for the non-corrected datasets. The limits of the shaded areas represent the minimum and maximum value of each parameter for the 0% biochar content.

the presence of biochar as revealed by Gao et al. (2019). In a field experimental design, the above-mentioned factors can be easily constrained notably through the investigation of the initial conditions. The physicochemical properties of biochar itself should also have a deep impact on soil polarization. Indeed, biochar can display a wide diversity in their initial physicochemical properties depending on feedstocks carbonization degree (depending on temperature and residence time) and particle size (Tomczyk et al., 2020). These factors are known to modify the the specific surface area of biochar (Leng et al., 2021) and therefore its surface conductivity.surface conductivity of biochar and/or the specific surface area (Leroy et al., 2017; Leng et al., 2021). Again, the initial properties of biochar can be constrained in a field experimental design in which the initial conditions are known. However, with time biochar is subjected to aging, which implies fragmentation as well as surface oxidation (Zeba et al., 2022). Aging therefore usually leads to a significant increase in the CEC while its effect on the specific surface area of biochar is not straightforward (L. Wang et al., 2020). As surface conduction is highly dependent on the CEC and specific surface area (see for instance: Leroy et al., 2008; Lévy et al., 2019; Mendieta et al., 2021), biochar aging should cause changes in the surface conduction. One could also expect that surface oxidation of biochar - implying a relative enrichment in carboxylic and phenolic groups (Wiedner et al., 2015) also affect surface conduction. Characterizing mineral wastes, Placencia-Gómez et al. (2013) observe a decrease in the phase shift with an increase in oxidation. Up to now, the effect of biochar aging on SIP signatures remains undocumented although biochar aging may drive the modifications of these signatures in the field. Following this, we suggest that SIP signatures measured in the field

following a time-lapse approach may be a suitable way to track processes involved in biochar aging.

4 Conclusion

We present a SIP dataset from natural soil and varying biochar concentration. Our data shows a clear relation between the Pelton parameters (ρ_0,m,c, and τ) and biochar content. Pelton parameters are traditionally used in geophysics and are a result of data processing. We propose simple parameters that directly relate to biochar content in a soil sample, such as: the mean phase from a middle frequency range (1.46 - 46.88 Hz), the phase at 11.7 Hz, and the shape parameter α. These parameters are simple to calculate and effective even with no high-frequency correction. Thus they could be a helpful tool in the field in order to possibly identify biochar hot-spots.

5 Funding declaration

-

6 Acknowledgements

We would like to thank Fayçal Rejiba for providing the soil samples used in these experiments, with their respective characterization.

7 Data availability

The dataset presented here is stored in a cloded access zenodo repository under the doi: 10.5281/zenodo.8090793. After acceptance of the paper it will be open access.

References

Aarts, E.H.L., Van Laarhoven, P. (1985). Statistical cooling: a general approach to combinatorial optimization problems. *Philips Journal of Research*, *40*(4), 193–226.

Atekwana, E. A., & Slater, L. D. (2009). Biogeophysics: A new frontier in Earth science research. *Reviews of Geophysics*, *47*(4), 1–30. doi: 10.1029/2009rg000285

Benech, C., Lombard, P., Rejiba, F., & Tabbagh, A. (2016). Demonstrating the contribution of dielectric permittivity to the in[U+2010]phase EMI response of soils: example from an archaeological site in Bahrain. *Near Surface Geophysics*, *14*(4), 337–344. doi: 10.3997/1873-0604.2016023

Binley, A., & Slater, L. (2020). *Resistivity and Induced Polarization: Theory and Applications to the Near-Surface Earth*. Cambridge University Press. Retrieved from `https://www.cambridge.org/core/product/identifier/9781108685955/type/book` doi: 10.1017/9781108685955

Brodowski, S., Amelung, W., Haumaier, L., Abetz, C., & Zech, W. (2005). Morphological and chemical properties of black carbon in physical soil fractions as revealed by scanning electron microscopy and energy-dispersive X-ray spectroscopy. *Geoderma*, *128*(1-2), 116–129. doi: 10.1016/j.geoderma.2004.12.019

Florsch, N., Revil, A., & Camerlynck, C. (2014). Inversion of generalized relaxation time distributions with optimized damping parameter. *Journal of Applied Geophysics*, *109*, 119–132. doi: 10.1016/j.jappgeo.2014.07.013

Friedman, S. P. (2005). Soil properties influencing apparent electrical conductivity:

A review. *Computers and Electronics in Agriculture*, *46*(1-3 SPEC. ISS.), 45–70. doi: 10.1016/j.compag.2004.11.001

Gao, Z., Haegel, F., Esser, O., Zimmermann, E., Vereecken, H., & Huisman, J. (2019). Spectral Induced Polarization of Biochar in Variably Saturated Soil. *Vadose Zone Journal*, *18*(1), 1–13. doi: 10.2136/vzj2018.12.0213

Gao, Z., Haegel, F. H., Huisman, J. A., Esser, O., Zimmermann, E., & Vereecken, H. (2017). Spectral induced polarization for the characterisation of biochar in sand. *Near Surface Geophysics*, *15*(6), 645–656. doi: 10.3997/1873-0604.2017045

Ghorbani, A., Cosenza, P., Revil, A., Zamora, M., Schmutz, M., Florsch, N., & Jougnot, D. (2009). Non-invasive monitoring of water content and textural changes in clay-rocks using spectral induced polarization: A laboratory investigation. *Applied Clay Science*, *43*(3), 493–502. doi: 10.1016/j.clay.2008.12.007

Glaser, B., Haumaier, L., Guggenberger, G., & Zech, W. (1998). Black carbon in soils: The use of benzenecarboxylic acids as specific markers. *Organic Geochemistry*, *29*(4), 811–819. doi: 10.1016/S0146-6380(98)00194-6

Gurin, G., Titov, K., Ilyin, Y., & Tarasov, A. (2014). Induced polarization of disseminated electronically conductive minerals: A semi-empirical model. *Geophysical Journal International*, *200*(3), 1555–1565. doi: 10.1093/gji/ggu490

Gustafsson, O., Haghseta, F., Chan, C., Macfarlane, J., & Gschwend, P., M. (1997). Quantification of the dilute sedimentary soot phase: Implications for PAH speciation and bioavailability. *Environmental Science and Technology*, *31*(1), 203–209. doi: 10.1021/es960317s

Haegel, F.-H., Zimmermann, E., D. Jablonowski, N., Esser, O., A. Huisman, J., & Vereecken, H. (2012). Application of Spectral Induced Polarization and Electrical Impedance Tomography on Mixtures of Biochars and Active Carbons with Sand. *25th Symposium on the Application of Geophpysics to Engineering & Environmental Problems*. doi: https://doi.org/10.3997/2214-4609-pdb.329.37

Hammes, K., & Schmidt, M. W. (2009). Changes of Biochar in Soil. In J. Lehmann & S. Joseph (Eds.), *Biochar for environmental management: Science and technology2* (1st ed., pp. 169–178). Routledge. doi: 10.4324/9781849770552

Hardy, B., Borchard, N., & Leifeld, J. (2022). Identification of thermal signature and quantification of charcoal in soil using differential scanning calorimetry and benzene polycarboxylic acid (BPCA) markers. *Soil*, *8*(2), 451–466. doi: 10.5194/soil-8-451-2022

Hermans, T., Goderniaux, P., Jougnot, D., Fleckenstein, J. H., Brunner, P., Nguyen, F., ... Le Borgne, T. (2023). Advancing measurements and representations of subsurface heterogeneity and dynamic processes: Towards 4D hydrogeology. *Hydrology and Earth System Sciences*, *27*(1), 255–287. doi: 10.5194/hess-27-255-2023

Joseph, S., Cowie, A. L., & Zwieten, L. V. (2021). How biochar works, and when it doesn't : A review of mechanisms controlling soil and plant responses to biochar. *GCB Bioenergy*, *13*, 1731–1764. doi: 10.1111/gcbb.12885

Kemna, A., Binley, A., Cassiani, G., Niederleithinger, E., Revil, A., Slater, L., ... Zimmermann, E. (2012). An overview of the spectral induced polarization method

for near-surface applications. *Near Surface Geophysics*, *10*(6), 453–468. doi: 10.3997/1873-0604.2012027

Kessouri, P., Furman, A., Huisman, J. A., Martin, T., Mellage, A., Ntarlagiannis, D., ... Placencia-Gomez, E. (2019). Induced polarization applied to biogeophysics: recent advances and future prospects. *Near Surface Geophysics*, *17*(6), 595–621. doi: 10.1002/nsg.12072

Knicker, H., Wiesmeier, M., & Dick, D. (2008). A simplified methods for the quantification of pyrogenic organic matter in grassland soils via chemical oxidation. *Geoderma*, *147*, 69–74. doi: 10.1016/j.geoderma.2008.07.008

Lehmann, J., Czimczik, C., Laird, D., & Sohi, S. (2009). Stability of Biochar in Soil. In J. Lehmann & S. Joseph (Eds.), *Biochar for environmental management: Science and technology* (1st ed., pp. 183–198). doi: 10.4324/9781849770552

Lehmann, J., & Joseph, S. (2015). *Biochar for environmental management: science, technology and implementation*. Routledge.

Leng, L., Xiong, Q., Yang, L., Li, H., Zhou, Y., Zhang, W., ... Huang, H. (2021). An overview on engineering the surface area and porosity of biochar. *Science of the Total Environment*, *763*, 144204. Retrieved from `https://doi.org/10.1016/j.scitotenv.2020.144204` doi: 10.1016/j.scitotenv.2020.144204

Leroy, P., Revil, A., Kemna, A., Cosenza, P., & Ghorbani, A. (2008). Complex conductivity of water-saturated packs of glass beads. *Journal of Colloid And Interface Science*, *321*, 103–117. doi: 10.1016/j.jcis.2007.12.031

Leroy, P., Weigand, M., Mériguet, G., Zimmermann, E., Tournassat, C., Fagerlund,

F., ... Alexander, J. (2017). Spectral induced polarization of Na-montmorillonite dispersions. *Journal of Colloid And Interface Science*, *505*, 1093–1110. doi: 10.1016/j.jcis.2017.06.071

Lesven, J., Druguet Dayras, M., Borne, R., Remy, C. C., Gillet, F., Bergeron, Y., ... Rius, D. (2022). Testing a new automated macrocharcoal detection method applied to a transect of lacustrine sediment cores in eastern Canada. *Quaternary Science Reviews*, *295*. doi: 10.1016/j.quascirev.2022.107780

Lévy, L., Weller, A., & Gibert, B. (2019). Influence of smectite and salinity on the imaginary and surface conductivity of volcanic rocks. *Near Surface Geophysics*, *17*(6), 653–673. doi: 10.1002/nsg.12069

Loewer, M., Günther, T., Igel, J., Kruschwitz, S., Martin, T., & Wagner, N. (2017). Ultra-broad-band electrical spectroscopy of soils and sediments-a combined permittivity and conductivity model. *Geophysical Journal International*, *210*(3), 1360–1373. doi: 10.1093/gji/ggx242

Maineult, A. (2016). Estimation of the electrical potential distribution along metallic casing from surface self-potential profile. *Journal of Applied Geophysics*, *129*, 66–78. doi: 10.1016/j.jappgeo.2016.03.038

Mao, D., & Revil, A. (2016). Induced polarization response of porous media with metallic particles - Part 3: A new approach to time-domain induced polarization tomography. *Geophysics*, *81*(4), D345–D357. doi: 10.1190/GEO2015-0283.1

Martin, T., Günther, T., Weller, A., & Kuhn, K. (2021). Classification of slag material by spectral induced polarization laboratory and field measurements. *Journal*

of Applied Geophysics, *194*(October 2020), 104439. Retrieved from https://doi.org/10.1016/j.jappgeo.2021.104439 doi: 10.1016/j.jappgeo.2021.104439

Mellage, A., Zakai, G., Efrati, B., Pagel, H., & Schwartz, N. (2022). Paraquat sorption- and organic matter-induced modifications of soil spectral induced polarization (SIP) signals. *Geophysical Journal International*, *229*(2), 1422–1433. doi: 10.1093/gji/ggab531

Mendieta, A., Jougnot, D., Leroy, P., & Maineult, A. (2021). Spectral induced polarization characterization of non[U+2010]consolidated clays for varying salinities [U+2010] an experimental study. *Journal of Geophysical Research: Solid Earth*, *126*(4). doi: 10.1029/2020jb021125

Mendieta, A., Maineult, A., Leroy, P., & Jougnot, D. (2023). Spectral induced polarization of heterogeneous non-consolidated clays. *Geophysical Journal International*, *233*, 436–447. doi: 10.1093/gji/ggac466

Mukherjee, S., Thakur, A. K., Goswami, R., Mazumder, P., Taki, K., Vithanage, M., & Kumar, M. (2021). Efficacy of agricultural waste derived biochar for arsenic removal: Tackling water quality in the Indo-Gangetic plain. *Journal of Environmental Management*, *281*(November 2020), 111814. doi: 10.1016/j.jenvman.2020.111814

Nakhli, S. A. A., Panta, S., Brown, J. D., Tian, J., & Imhoff, P. T. (2019). Quantifying biochar content in a field soil with varying organic matter content using a two-temperature loss on ignition method. *Science of the Total Environment*, *658*, 1106–1116. Retrieved from https://doi.org/10.1016/

j.scitotenv.2018.12.174 doi: 10.1016/j.scitotenv.2018.12.174

Paetsch, L., Mueller, C. W., Rumpel, C., Angst, Š., Wiesheu, A. C., Girardin, C., ... Kögel-knabner, I. (2017). A multi-technique approach to assess the fate of biochar in soil and to quantify its effect on soil organic matter composition. *Organic Geochemistry*, *112*, 177–186. doi: 10.1016/j.orggeochem.2017.06.012

Palansooriya, K. N., Wong, J. T. F., Hashimoto, Y., Huang, L., Rinklebe, J., Chang, S. X., ... Ok, Y. S. (2019). Response of microbial communities to biochar - amended soils: a critical review. *Biochar*, *1*, 3–22. doi: 10.1007/s42773-019-00009-2

Parsekian, A., Singha, K., Minsley, B., Holbrook, W. S., & Slater, L. (2015). Multiscale geophysical imaging of the critical zone. *Reviews of Geophysics*, *532*, 1–26. doi: 10.1002/2014RG000465

Placencia-Gómez, E., Slater, L., Ntarlagiannis, D., & Binley, A. (2013). Laboratory SIP signatures associated with oxidation of disseminated metal sulfides. *Journal of Contaminant Hydrology*, *148*, 25–38. doi: 10.1016/j.jconhyd.2013.02.007

Revil, A., Karaoulis, M., Johnson, T., & Kemna, A. (2012). Review : Some low-frequency electrical methods for subsurface characterization and monitoring in hydrogeology. *Hydrogeology Journal*, *20*, 617–658. doi: 10.1007/s10040-011-0819-x

Revil, A., Sleevi, M., & Mao, D. (2017). Induced polarization response of porous media with metallic particles - part 5: Influence of the background polarization. *Geophysics*, *82*(2), E77–E96. doi: 10.1190/GEO2016-0388.1

Rhodes, A. N. (1998). A method for the preparation and quantification of micro-

scopic charcoal from terrestrial and lacustrine sediment cores. *The Holocene*, *8*(1), 113–117. doi: 10.1191/095968398671104653

Roberts, K. G., Gloy, B. A., Joseph, S., Scott, N. R., & Lehmann, J. (2010). Life cycle assessment of biochar systems: Estimating the energetic, economic, and climate change potential. *Environmental Science and Technology*, *44*(2), 827–833. doi: 10.1021/es902266r

Robinson, D., Binley, A., Crook, N., Day-Lewis, F., Ferré, T., Grauch, V., ... Slater, L. (2008). Advancing process-based watershed hydrological research using near-surface geophysics: a vision for, and review of, electrical and magnetic geophysical methods. *Hydrological Processes*, *22*, 3604–3636. doi: 10.1002/hyp.6963

Samouëlian, A., Cousin, I., Tabbagh, A., Bruand, A., & Richard, G. (2005). Electrical resistivity survey in soil science: A review. *Soil and Tillage Research*, *83*(2), 173–193. doi: 10.1016/j.still.2004.10.004

Schwartz, N., Shalem, T., & Furman, A. (2014). The effect of organic acid on the spectral-induced polarization response of soil. *Geophysical Journal International*, *197*(1), 269–276. doi: 10.1093/gji/ggt529

Singh, R., Babu, J. N., Kumar, R., Srivastava, P., Singh, P., & Raghubanshi, A. S. (2015). Multifaceted application of crop residue biochar as a tool for sustainable agriculture: An ecological perspective. *Ecological Engineering*, *77*, 324–347. doi: 10.1016/j.ecoleng.2015.01.011

Skjemstad, J., Clarke, P., Taylor, J., Oades, J., & Mcclure, S. (1996). The chemistry and nature of protected carbon in soil. *Soil Reasearch*, *34*, 251–271. doi: 10.1071/

SR9960251

Strobel, C., Dorrich, M., Cirpka, O. A., Huisman, J. A., & Mellage, A. (2023). Organic matter matters - The imaginary conductivity of sediments rich in solid organic carbon. In *Egu general assembly 2023.* doi: 10.5194/egusphere-egu23-1838

Tabbagh, A., Rejiba, F., Finco, C., Schamper, C., Souffaché, B., Camerlynck, C., ... Maineult, A. (2021). The case for considering polarization in the interpretation of electrical and electromagnetic measurements in the 3 kHz to 3 MHz frequency range. *Surveys in Geophysics*, *42*, 377–397. doi: 10.1007/s10712-020-09625-1

Tarasov, A., & Titov, K. (2013). On the use of the Cole-Cole equations in spectral induced polarization. *Geophysical Journal International*, *195*, 352–356. doi: 10.1093/gji/ggt251

Tomczyk, A., Sokołowska, Z., & Boguta, P. (2020). Biochar physicochemical properties: pyrolysis temperature and feedstock kind effects. *Reviews in Environmental Science and Biotechnology*, *19*(1), 191–215. doi: 10.1007/s11157-020-09523-3

Wang, J., & Wang, S. (2019). Preparation, modification and environmental application of biochar: A review. *Journal of Cleaner Production*, *227*, 1002–1022. Retrieved from `https://doi.org/10.1016/j.jclepro.2019.04.282` doi: 10.1016/j.jclepro.2019.04.282

Wang, L., O'Connor, D., Rinklebe, J., Ok, Y. S., Tsang, D. C., Shen, Z., & Hou, D. (2020). Biochar Aging: Mechanisms, Physicochemical Changes, Assessment, and Implications for Field Applications. *Environmental Science and Technology*, *54*(23), 14797–14814. doi: 10.1021/acs.est.0c04033

494 Weller, A., & Slater, L. (2022). Ambiguity in induced polarization time constants
495 and the advantage of the Pelton model. *Geophysics*, *87*(6), E393–E399. doi: 10
496 .1190/geo2022-0158.1
497 Wiedner, K., Fischer, D., Walther, S., Criscuoli, I., Favilli, F., Nelle, O., & Glaser,
498 B. (2015). Acceleration of Biochar Surface Oxidation during Compost-
499 ing? *Journal of Agricultural and Food Chemistry*, *63*(15), 3830–3837. doi:
500 10.1021/acs.jafc.5b00846
501 Woolf, D., Amonette, J. E., Street-Perrott, F. A., Lehmann, J., & Joseph, S. (2010).
502 Sustainable biochar to mitigate global climate change. *Nature Communications*,
503 *1*(5). doi: 10.1038/ncomms1053
504 Xu, Z., He, M., Xu, X., Cao, X., & Tsang, D. C. (2021). Impacts of different acti-
505 vation processes on the carbon stability of biochar for oxidation resistance. *Biore-*
506 *source Technology*, *338*(July), 125555. doi: 10.1016/j.biortech.2021.125555
507 Yang, F., Zuo, X., Zhou, Y., Wu, S., & Wang, M. (2022). Stability of biochar in five
508 soils : Effects from soil property. *Environmental progress and Sustainable Energy*,
509 *41*, 1–9. doi: 10.1002/ep.13775
510 Zeba, N., Berry, T. D., Panke-Buisse, K., & Whitman, T. (2022). Effects of
511 physical, chemical, and biological ageing on the mineralization of pine wood
512 biochar by a Streptomyces isolate. *PLoS ONE*, *17*(4 April), 1–18. doi:
513 10.1371/journal.pone.0265663
514 Zhang, W., Niu, J., Morales, V. L., Chen, X., Hay, A. G., Lehmann, J., & Steen-
515 huis, T. S. (2010). Transport and retention of biochar particles in porous media

: effect of pH , ionic strength , and particle size. *Ecohydrology*, *3*, 497–508. doi: 10.1002/eco

Zimmermann, E., Kemna, A., Berwix, J., Glaas, W., Münch, H. M., & Huisman, J. A. (2008). A high-accuracy impedance spectrometer for measuring sediments with low polarizability. *Measurement Science and Technology*, *19*(10), 1–9. doi: 10.1088/0957-0233/19/10/105603

8 Appendix 1

We define three frequencies namely the lowest frequency of interest (LF),intermediate frequency of interest (IF) and highest frequency of interest (HF). the only need in our case is that LF<IF<HF. This triad of frequencies defines a triad of values on the curve defining a triangle. The parameter α is determined as the scalar product between the unitary vector defined by the couple (LF, HF) rotated by $\frac{\pi}{2}$ and the vector corresponding to the height of the triangle associated with the side (LF,HF) oriented from the side to the point corresponding to MF. If this product is positive, then the curves exhibit a concave shape on the frequency domain chosen. on the other hand, if α is negative then the curve exhibit a convex shape on the frequency domain chosen. In addition, the amplitude gives a hint on the strength of the effect.

Four points are necessary to compute the α parameter :

$$A = \begin{pmatrix} x_{LF} \\ y_{LF} \end{pmatrix}, B = \begin{pmatrix} x_{IF} \\ y_{IF} \end{pmatrix}, C = \begin{pmatrix} x_{HF} \\ y_{HF} \end{pmatrix}, O = \begin{pmatrix} x \\ y \end{pmatrix} \tag{2}$$

The O point is as the intercept between the line (AC) and a perpendicular passing by B. Hence we can define O as the point which coordinate verify :

$$\begin{cases} y = ax + b \\ \\ y = -\frac{x}{a} + \beta \end{cases} \tag{3}$$

with :

$$a = \frac{y_{HF} - y_{LF}}{x_{HF} - x_{LF}} \tag{4}$$

$$b = \frac{y_{LF}x_{HF} - y_{HF}x_{LF}}{x_{HF} - x_{LF}} \tag{5}$$

$$\beta = y_{IF} + \frac{x_{IF}}{a} \tag{6}$$

Given the x and y values obtained the α parameter is computed as :

$$\alpha = \vec{OB}.\frac{\vec{AC}_{\perp}}{\|\vec{AC}\|} \tag{7}$$

where

$$\vec{OB} = \begin{pmatrix} x_{IF} - x \\ y_{IF} - y \end{pmatrix} \tag{8}$$

$$\vec{AC} = \begin{pmatrix} x_{HF} - x_{LF} \\ y_{HF} - y_{LF} \end{pmatrix} \tag{9}$$

$$\vec{AC}_{\perp} = \begin{pmatrix} y_{LF} - y_{HF} \\ x_{HF} - x_{LF} \end{pmatrix} \tag{10}$$

9 Appendix 2

A correction for the high frequency noise was applied to the SIP data. The applied procedure is the following:

According to the Debye decomposition, a complex conductivity spectra $\sigma*(\omega)$ can be written in the form,

$$\frac{\sigma^*(\omega) - \sigma_\infty}{\sigma_0 - \sigma_\infty} = \sum_{k=1}^{N} \frac{m_k}{1 + i\omega\tau_k}, \tag{11}$$

where ω is the angular frequency (in mrad), equals to $2\pi f$, with frequency f, σ_∞ is the amplitude of the conductivity at an infinite frequency, and σ_0 is the amplitude of the conductivity at a null frequency, and with $\tau_k = 1/(2\pi f_k)$, with f_k, $k = 1, ..., N$ a sampling of the used frequency range.

Therefore:

$$\sigma^*(\omega) = \sigma_\infty + (\sigma_0 - \sigma_\infty) \sum_{k=1}^{N} \frac{m_k}{1 + i\omega\tau_k}. \tag{12}$$

This formulation does not take into account the divergence of the signature that can be observed at high frequencies (>100-1000 Hz), linked to a natural dielectric component or to electromagnetic coupling effects (e.g., Florsch et al., 2014). It is therefore necessary to add a term to equation 12 to account for this response, namely $i\omega C$, where C is a capacitance.

On the other hand, it is impossible to determine independently $(\sigma_0 - \sigma_\infty)$ and m_k. We propose then to replace equation 12 with:

$$\sigma^*(\omega) = \sigma_\infty + M \sum_{k=1}^{N} \frac{m_k}{1 + i\omega\tau_k} + i\omega C, \tag{13}$$

where M is a positive constant.

The values of σ_∞, M, m_k for $k = 1, ..., N$ and C are searched by optimization, using the simulated annealing algorithm (see Aarts, E.H.L., Van Laarhoven, 1985; Maineult, 2016, for its implementation), so as to minimize the fit coefficient between the spectrum predicted by equation 13 (calculated at frequencies f_k,$k = 1, ..., N$) and the whole set of measurements $[f_k,\sigma_k^*]$,$k = 1, ..., N$.

Once these parameters are determined, the measured spectrum corrected for high frequency disturbances is expressed by:

$$\tilde{\sigma_k^*} = \sigma_k^* - i\omega C \tag{14}$$

for $k = 1, ..., N$.